

Suppression of Hepatic Inflammation *via* Systemic siRNA Delivery by Membrane-Disruptive and Endosomolytic Helical Polypeptide Hybrid Nanoparticles

Hua He,[†] Nan Zheng,[‡] Ziyuan Song,[‡] Kyung Hoon Kim,[‡] Catherine Yao,[‡] Rujing Zhang,[‡] Chenglin Zhang,[§] Yuhui Huang,[§] Fatih M. Uckun,[⊥] Jianjun Cheng,[‡] Yanfeng Zhang,^{||} and Lichen Yin^{*,†}

[†]Institute of Functional Nano & Soft Materials (FUNSOM), Jiangsu Key Laboratory for Carbon-Based Functional Materials & Devices, Soochow University, 199 Ren'ai Road, Suzhou 215123, China

[‡]Department of Materials Science and Engineering, University of Illinois at Urbana—Champaign, 1304 West Green Street, Urbana, Illinois 61801, United States

[§]The Cyrus Tang Hematology Center, The Collaborative Innovation Center of Hematology, Soochow University, Suzhou 215123, China

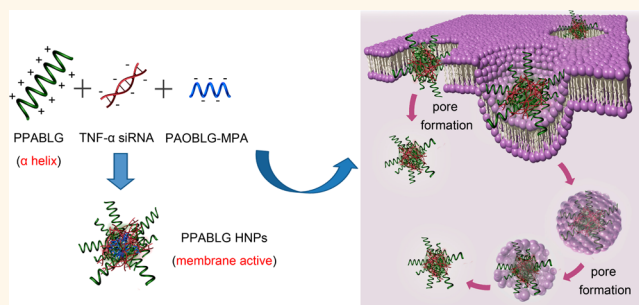
[⊥]Division of Hematology-Oncology, Systems Immunobiology Laboratory, Children's Center for Cancer and Blood Diseases, Children's Hospital, Los Angeles, California 90027, United States

^{||}Department of Applied Chemistry, School of Science, Xi'an Jiaotong University, Xi'an 710049, China

Supporting Information

ABSTRACT: Treatment of inflammatory diseases represents one of the biggest clinical challenges. RNA interference (RNAi) against TNF- α provides a promising modality toward anti-inflammation therapy, but its therapeutic potential is greatly hampered by the lack of efficient siRNA delivery vehicles *in vivo*. Herein, we report a hybrid nanoparticulate (HNP) system based on a cationic helical polypeptide PPABLG for the efficient delivery of TNF- α siRNA. The helical structure of PPABLG features pore formation on cellular and endosomal membranes to facilitate the direct translocation as well as endosomal escape of TNF- α siRNA in macrophages, representing a unique superiority to a majority of the existing polycation-based gene vectors that experience severe endosomal entrapment and lysosomal degradation. As such, HNPs containing TNF- α siRNA afforded effective systemic TNF- α knockdown following systemic administration at a low dose of 50 μ g of siRNA/kg and thus demonstrated a potent anti-inflammatory effect to rescue animals from LPS/D-GalN-induced hepatic sepsis. This study therefore verifies that the bioactive secondary structure of polypeptides significantly dominates the *in vivo* siRNA delivery efficiency, and the unique properties of PPABLG HNPs render remarkable potentials for anti-inflammation therapies.

KEYWORDS: siRNA delivery, helical polypeptide, membrane disruption, endosomal escape, TNF- α , anti-inflammation therapy



Inflammatory diseases, such as rheumatoid arthritis, inflammatory bowel diseases (*e.g.*, Crohn's disease), and septic shock are a group of dysregulated inflammatory responses which represent one of the biggest clinical challenges.^{1,2} Overproduction of tumor necrosis factor- α (TNF- α), a pro-inflammatory cytokine secreted by systemically derived macrophages, is dominantly associated with the development and pathogenesis of inflammatory diseases.³ In current clinical settings, anti-TNF- α immunotherapy using TNF- α monoclonal antibodies, receptors, or inhibitors provides

the basis for the treatment against inflammatory disorders.⁴ Nonetheless, these anti-TNF- α therapies often suffer from high cost, autoimmunity to antibodies, and adverse effects associated with chronic inhibitor treatment.⁵ It therefore necessitates the development of new methods to mediate therapeutic TNF- α suppression toward anti-inflammatory outcomes.

Received: August 31, 2015

Accepted: January 20, 2016

Published: January 26, 2016

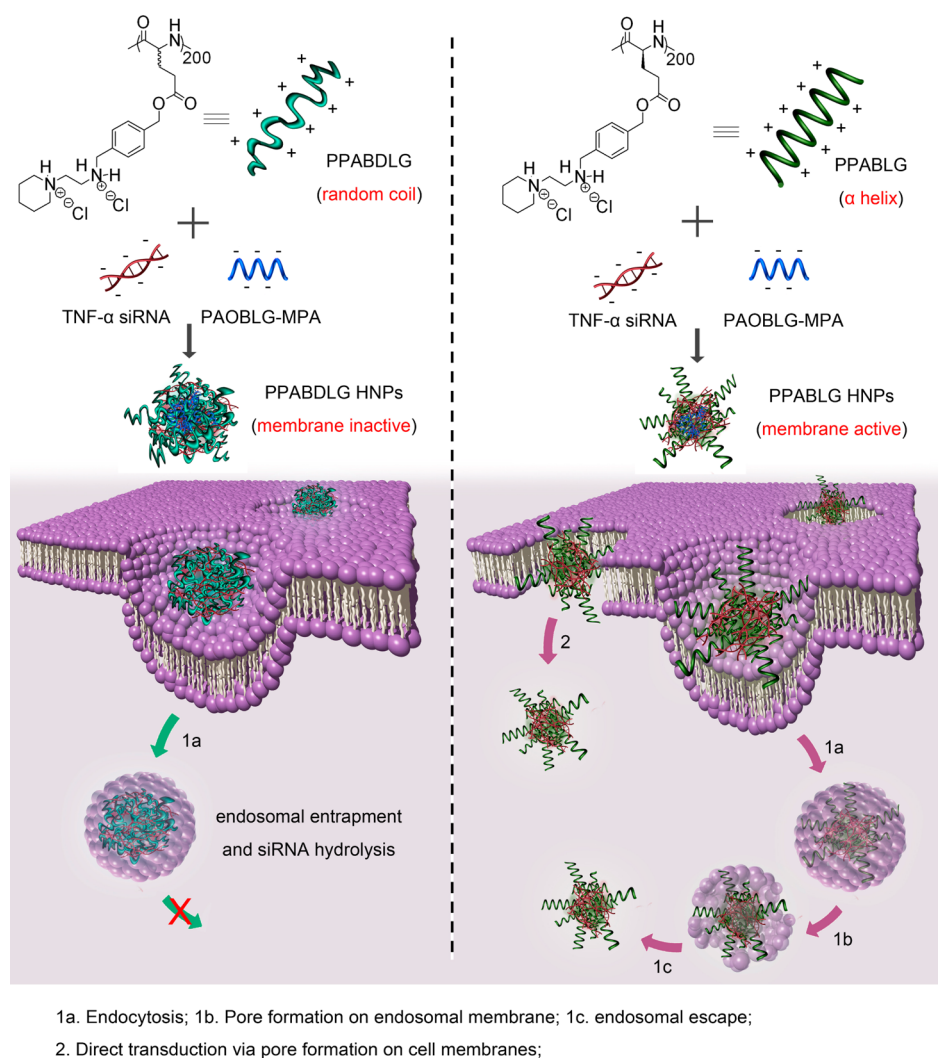


Figure 1. Intracellular kinetics of PPABLG/PAOBLG-MPA/siRNA and PPABDLG/PAOBLG-MPA/siRNA HNPs, highlighting the helicity-dependent membrane disruption capabilities of PPABLG toward effective cellular internalization as well as endosomal escape.

RNA interference (RNAi) mediated by small interfering RNA (siRNA) is an important mechanism that regulates gene expression in eukaryotic cells *via* site-specific mRNA cleavage and degradation. Because of its efficiency and sequence specificity, the RNAi machinery affords an exciting modality for the treatment of a vast array of human diseases.^{6–15} As such, siRNA delivery to macrophages to attenuate TNF- α production provides an alternative strategy toward anti-inflammatory therapy.^{16–21} Nevertheless, the transformative potential of RNAi has been hampered by various systemic barriers, such as the nuclease-assisted siRNA degradation, minimal intracellular delivery across cell membranes, and endosomal/lysosomal entrapment.^{22,23} In order to circumvent these barriers, a variety of vectors and methods have been developed, among which cell-penetrating peptides (CPPs) with unique membrane activities are widely utilized to promote the cellular internalization as well as endosomal escape of the siRNA cargos.^{24–27} Well-known examples of CPPs include oligoarginine, HIV-TAT, penetratin, transportin, and melittin.²⁸ Helical structure is often observed in CPPs or formed in CPPs during the course of membrane transduction, which presents a rigid amphiphilic structure to interact with and destabilize the lipid bilayers, thus creating transient pathways to facilitate translocation of

exogenous materials.^{29–31} However, CPPs are often short (<30 residues) and lack adequate cationic charge density to effectively condense siRNA by themselves. Additionally, after complexing with the siRNA molecules, the overall positive charge of CPPs may be neutralized, thus reducing their affinities with negatively charged cell surfaces to decrease the membrane activities as well as transfection ability.^{32,33} As such, CPPs often serve as membrane-active ligands to improve the delivery efficiencies of existing systems.^{34,35}

To address the shortcomings of CPPs, we herein developed hybrid nanoparticles (HNPs) based on a cationic helical polypeptide PPABLG for the efficient delivery of TNF- α siRNA toward anti-inflammation therapies. The stabilized helical structure of PPABLG features potent membrane activities, while the high molecular weight and high cationic charge density allow it to maintain strong membrane destabilization/disruption capacities after siRNA condensation. As such, effective cellular internalization and endosomal escape of the siRNA cargo would be allowed (Figure 1). The capability of HNPs to mediate intracellular siRNA delivery and induce TNF- α knockdown was evaluated in murine macrophages *in vitro*, and the essential roles of helical secondary structure in dominating intracellular kinetics were mechanically probed.

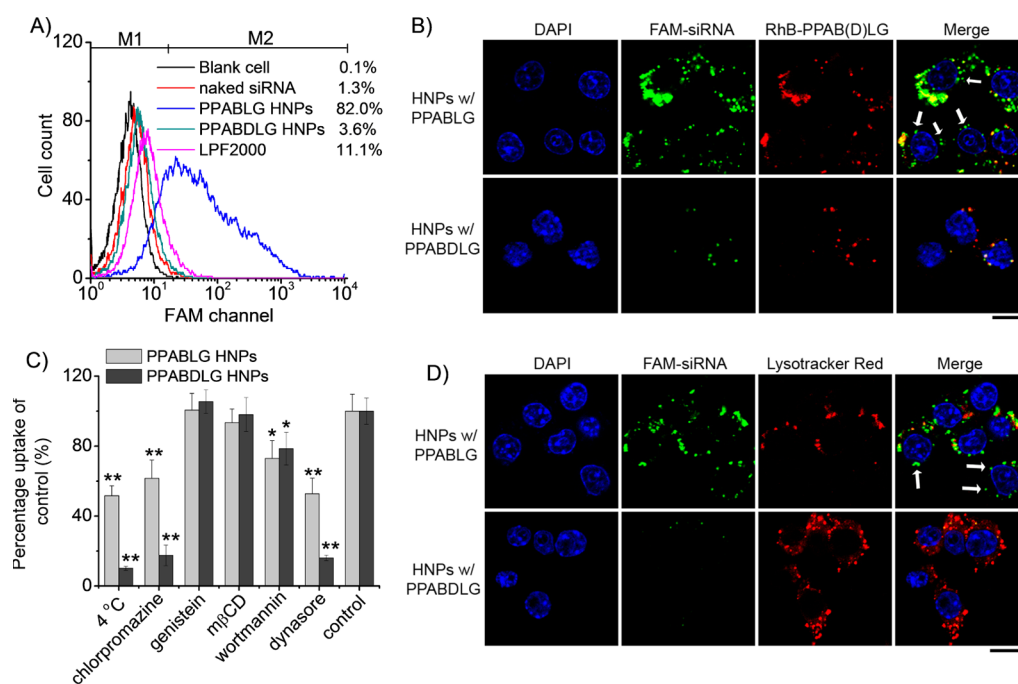


Figure 2. HNPs efficiently deliver TNF- α siRNA into macrophages *in vitro*. (A) Flow cytometric analyses of RAW 264.7 cells after 4 h incubation with HNPs containing FAM-siRNA. Nontreated cells served as the blank. (B) CLSM images of RAW 264.7 cells following 4 h incubation with HNPs composed of RhB-PPABLG and FAM-siRNA. (C) Mechanistic probes of the internalization pathways of HNPs in RAW 264.7 cells by monitoring the cell uptake level of FAM-siRNA in the presence of various endocytic inhibitors ($n = 3$). (D) CLSM images of RAW 264.7 cells treated with HNPs containing FAM-siRNA for 4 h and stained with LysoTracker Red. Scale bar = 20 μm . White arrows indicate the separation of green fluorescence from red fluorescence.

In a lipopolysaccharide (LPS)-induced hepatic inflammation model, the systemic gene-silencing efficiency as well as the anti-inflammatory efficiency of *i.v.*-injected HNPs was further evaluated.

RESULTS AND DISCUSSION

PPABLG was first synthesized *via* controlled ring-opening polymerization of γ -(4-vinylbenzyl)-L-glutamate NCA (VB-L-Glu-NCA), as initiated by hexamethyldisilazane (HMDS) followed by multistep side-chain modification.^{36,37} The resulting polypeptide showed a well-defined degree of polymerization of 206 and low polydispersity index (PDI = 1.08) as determined by gel permeation chromatography (GPC). By maintaining an 11- σ bond distance between the peptide backbone and the side-chain-charged amine groups, the intramolecular charge repulsion was minimized, and thus the polypeptides adopted a typical α -helical secondary structure in aqueous solutions, as evidenced by the characteristic negative ellipticity of minima at 208 and 222 nm in the circular dichroism (CD) spectrum (Supporting Information Figure S4). The helicity of PPABLG was stable within the pH range of 2–9, salt concentration of 0.05–1 M, and urea concentration of 0–4 M (Figure S5). Additionally, following a 2 h treatment with trypsin at various concentrations, the PPABLG was also allowed to maintain its helical structure (Figure S5), further suggesting its desired stability in terms of helicity. As such, the polypeptide should be able to maintain helicity-dependent membrane activities at both neutral extracellular pH and acidic endosomal/lysosomal pH to enable cellular internalization as well as endosomal escape. Because siRNA is short (21–23 bp) and linear, its electrostatic interactions with polycations are often weak.³⁸ Therefore, we incorporated another anionic polypeptide, PAOBLG-MPA,³⁹ to strengthen the interactions

with the cationic PPABLG and simultaneously promote the TNF- α siRNA encapsulation in the complex structure.⁴⁰ The siRNA condensation was confirmed by the gel retardation assay, as evidenced by the inhibited siRNA migration in the 4% agarose gel after electrophoresis (Figure S6). An increase in the PPABLG/PAOBLG-MPA ratio led to notably decreased particle size and increased ζ -potential; at the optimal PPABLG/PAOBLG-MPA/TNF- α siRNA weight ratio of 20/2/1, the complexes demonstrated an average diameter of \sim 100 nm, PDI of 0.197, positive ζ -potential of \sim 30 mV, and high siRNA condensation efficiency of 97.4% (Figures S7 and S8). Following incubation with DMEM containing 10% fetal bovine serum (FBS) for 2 h, the particle size of PPABLG HNPs slightly increased to \sim 190 nm, which could be attributed to the coverage of serum proteins on particle surfaces. Such formulation was used afterward for *in vitro* and *in vivo* studies. Additionally, PPABLG was able to maintain helical structure after condensing siRNA to form complexes (Figure S4), which would allow the polypeptide to preserve its helicity-dependent membrane activities. After dilution with PBS for 10-fold, particle size and ζ -potential of HNPs remained unaltered (data not shown), indicating desired stability of HNPs against salt and dilution.

Since macrophages are the target cells for TNF- α siRNA-mediated gene silencing, we first explored the *in vitro* siRNA delivery efficiency of HNPs (PPABLG/PAOBLG-MPA/siRNA = 20/2/1, w/w/w) in murine macrophages, RAW 264.7 cells. Flow cytometric analysis revealed that PPABLG HNPs markedly increased the cellular uptake level of FAM-siRNA that was internalized by over 80% of the cells after a 4 h incubation at 37 °C (Figure 2A). In direct comparison, commercial transfection reagent Lipofectamine 2000 (LPF2000) exhibited a notably lower uptake level (\sim 10%).

Additionally, even after a short (0.5 h) incubation time under shaking (100 rpm), PPABLG HNPs led to an appreciable cellular uptake level of FAM-siRNA (Figure S9), which indicated that PPABLG HNP-mediated cellular internalization was a rapid and efficient process, mainly due to the potent membrane permeability of the helical polypeptide. Confocal laser scanning microscopy (CLSM) observation further evidenced the extensive cellular internalization of HNPs composed of rhodamine (RhB)-labeled PPABLG and FAM-siRNA (Figure 2B). Separation of green fluorescence (FAM-siRNA) from red fluorescence (RhB-PPABLG) was noted, indicating that siRNA could be released from the HNPs in the cytoplasm to allow binding to the target mRNA. When PPABLG was replaced by its random-coiled analogue—PPABDLG synthesized from the racemic D,L-Glu NCA—the siRNA delivery efficiency of HNPs (PPABDLG/PAOBLG-MPA/siRNA = 20/2/1, w/w/w) was largely compromised (Figure 2A,B), which could be attributed to the loss of helix-dependent membrane activity of the polypeptide.

The success of nonviral gene transfection is closely related to the intracellular kinetics, such as the transmembrane trafficking pathway and endosomal/lysosomal entrapment. Therefore, we mechanically probed the capabilities of HNPs to overcome these cellular barriers. We first explored the internalization pathways of HNPs in macrophages by monitoring the cell uptake level at low temperature (4 °C) or in the presence of various endocytic inhibitors. As shown in Figure 2C, the cellular uptake level of PPABLG HNPs was reduced by only 50% at 4 °C when energy-dependent endocytosis was blocked. It therefore indicated that a substantial amount of HNPs entered the cells *via* energy-independent non-endocytosis pathways. Such results were in accord with the CLSM observation, wherein the cytoplasmic distribution of FAM-siRNA revealed both punctated and permeated patterns that corresponded to endocytic vesicles and non-endocytic permeation, respectively (Figure 2D and Figure S12).⁴¹ In comparison, the uptake level of PPABDLG HNPs was inhibited by ~90% at 4 °C (Figure 2C), suggesting that the majority of them were endocytosed into the cells. Such discrepancy between the PPABLG and PPABDLG HNPs highlighted the essential roles of the helical secondary structure of the polypeptide to mediate direct translocation of cargo siRNA across cell membranes. To elucidate such a hypothesis, we further evaluated the capabilities of PPABLG or PPABDLG HNPs to mediate pore formation on cell membranes by monitoring the cell uptake of fluorescein isothiocyanate (FITC) in its nonreactive form after reaction with Tris (abbreviated as FITC-Tris), a hydrophilic membrane-impermeable fluorescent dye.⁴¹ FITC-Tris was negligibly taken up by cells, due to its impermeability across intact membranes. After co-incubation with PPABLG HNPs, FITC-Tris uptake was dramatically enhanced by ~200-fold, while following co-incubation with PPABDLG HNPs, FITC-Tris uptake level only increased by ~5-fold, which was similar to Arg9 and Tat (Figure S11). It therefore demonstrated that the helical PPABLG, but not the random-coiled PPABDLG, was able to induce pore formation on cell membranes to allow direct translocation of siRNA. When compared to free PPABLG, HNPs showed only slightly reduced pore formation capacity, which substantiated that the membrane permeability of PPABLG was well-maintained after siRNA condensation, presumably due to its sufficiently long backbone that allowed exposure of the helical motif on the nanoparticle surface. While the pores PPABLG punctured may not easily allow the

diffusion of nanoparticles with diameters larger than 100 nm, the membrane-permeable PPABLG can be extruded into the phospholipid bilayers to mediate close contact between HNPs and lipid bilayers. Upon contact with a large amount of the negatively charged components in the lipid bilayers, some siRNA may be competitively released toward the localized lipid area, and these siRNA molecules might be able to subsequently diffuse into the cytoplasm through the pores that PPABLG had created.

The internalization pathway is closely related to the intracellular fate, which ultimately dominates the RNAi efficiency. For instance, clathrin-mediated endocytosis (CME) often leads to endosomal entrapment and lysosomal degradation of the generic cargo, thus resulting in low RNAi efficiency unless the delivery vector is able to trigger effective endosomal escape.⁴² Comparatively, caveolae is a nonacidic and non-digestive route, avoiding endosomal entrapment and facilitating direct transport to the Golgi or endoplasmic reticulum.⁴² For PPABLG HNPs, the uptake level was reduced by only ~50% in the presence of CME inhibitor chlorpromazine, while caveolae inhibitor genistein and macropinocytosis inhibitor wortmannin exerted an unappreciable inhibitory effect (Figure 2C). CLSM observation accorded well with such a result, in that internalized PPABLG HNPs colocalized with transferrin-Alexa Fluor 633 that was taken up *via* CME while they did not colocalize with FITC-CTB that was taken up *via* caveolae (Figure S14).^{42–44} Comparatively, PPABDLG HNPs experienced a 90% reduction in the uptake level in the presence of chlorpromazine, while genistein and m β CD showed unappreciable inhibitory effect, indicating involvement of CME rather than caveolae. Wortmannin showed a slight inhibitory effect, which indicated that macropinocytosis was only partially involved. These disparities between PPABLG and PPABDLG HNPs again substantiated that, by effectively mediating direct membrane translocation, the helical conformation of the polypeptide played critical roles in evading the CME pathway, which could potentially lead to avoidance of endosomal/lysosomal entrapment and efficient gene transfection. In support of such a hypothesis, we further probed the endosomal/lysosomal entrapment of HNPs by visualizing and quantifying the colocalization of the FAM-siRNA-containing HNPs and Lysotracker-Red-stained endosomes/lysosomes. As depicted in Figure 2D, internalized PPABDLG HNPs (green fluorescence of FAM-siRNA) completely colocalized with endosomes/lysosomes (red fluorescence), indicating that they experienced severe endosomal entrapment. Comparatively, PPABLG effectively bypassed the entrapment by late endosomes/lysosomes, evidenced by the notable separation of green fluorescence from red fluorescence. Consistent with such an observation, PPABLG showed a notably lower colocalization ratio between FAM-siRNA and Lysotracker-Red-stained endosomes than PPABDLG (Figure S13), which again substantiated the capacity of the helical polypeptide but not the random-coiled polypeptide to mediate effective endosomal escape.

Upon identifying the unique properties of PPABLG HNPs in overcoming intracellular barriers against RNAi, we then evaluated the TNF- α knockdown efficiency *in vitro* in RAW 264.7 cells. As shown in Figure S15, PPABLG HNPs (PPABLG/PAOBLG-MPA/siRNA = 20/2/1, w/w/w) notably inhibited LPS-induced TNF- α production in RAW 264.7 cells by ~90% at the siRNA concentration of 0.2 μ g/mL. As controls, PPABLG HNPs containing Scr siRNA and naked TNF- α siRNA showed negligible gene-silencing effect. The

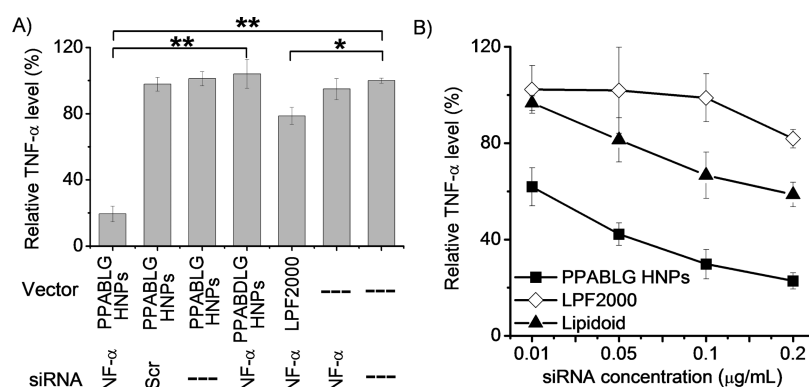


Figure 3. HNPs mediate effective TNF- α silencing in murine primary macrophages. (A) TNF- α level of PECs following treatment with HNPs for 4 h at 0.2 μg of siRNA/mL in DMEM containing 10% FBS, incubation in fresh media for 20 h, and subsequent LPS stimulation at 100 ng/mL for 5 h ($n = 3$). (B) TNF- α levels of PECs following treatment with HNPs, LPF2000/siRNA complexes, or lipidoid/siRNA complexes at various siRNA doses in DMEM containing 10% FBS ($n = 3$).

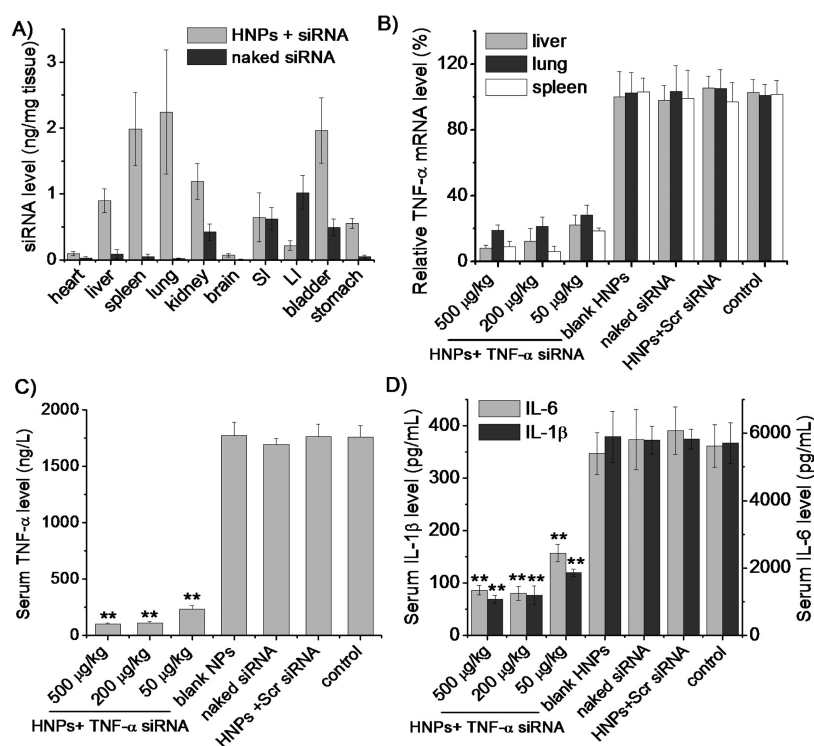


Figure 4. Systemically administered HNPs attenuate systemic TNF- α production as induced by LPS/D-GalN. (A) Biodistribution profiles of DY800-siRNA in mice 2 h after i.v. injection of DY800-siRNA-containing HNPs or naked DY800-siRNA ($n = 3$). SI and LI referred to small intestine and large intestine, respectively. (B) Relative TNF- α mRNA levels in mouse liver, spleen, and lung 24 h after i.v. injection of HNPs ($n = 4$). LPS and D-GalN (100 $\mu\text{g/kg}$ and 1.25 g/kg) were i.p.-injected 5 h prior to organ harvest. Serum levels of pro-inflammatory cytokines, TNF- α (C) and IL-1 β /IL-6 (D), in mice receiving i.v. administration of HNPs. LPS/D-GalN was i.p.-injected 24 h after administration, and serum TNF- α , IL-1 β , and IL-6 levels were quantified 1.5 h later by ELISA ($n = 4$).

intracellular TNF- α mRNA level was also monitored by real-time polymerase chain reaction (PCR) (Figure S16), which confirmed the siRNA-mediated sequence-specific cleavage of mRNA. In agreement with their low cellular internalization level and weak capability in mediating endosomal escape, PPABDLG HNPs did not evoke an appreciable knock-down effect. PPABLG HNPs remarkably outperformed commercial reagent LPF2000 in terms of TNF- α gene-silencing efficiency, achieving comparable knock-down efficiency ($\sim 40\%$) to LPF2000 at a 4-fold lower siRNA dose (Figure S17). To more reflect the physiologically relevant conditions, we also assessed the silencing efficiency of HNPs against TNF- α in

murine peritoneal exudate cells (PECs) as primary macrophages in the presence of 10% serum. The potent silencing efficiency of PPABLG HNPs was again substantiated, which inhibited TNF- α production by $\sim 70\%$ at the siRNA concentration of 0.2 $\mu\text{g/mL}$ and substantially outperformed LPF2000 as the commercial reagent and lipidoid (structure shown in Scheme S3) as one of the well-established delivery systems⁴⁵ (Figure 3A,B). While RAW 264.7 cells and murine PECs were herein used as representative macrophage cell lines for exploring the intracellular kinetics as well as gene-silencing efficiencies of PPABLG HNPs, it has to be noted that they may not completely replicate Kupffer cells as the target cells during

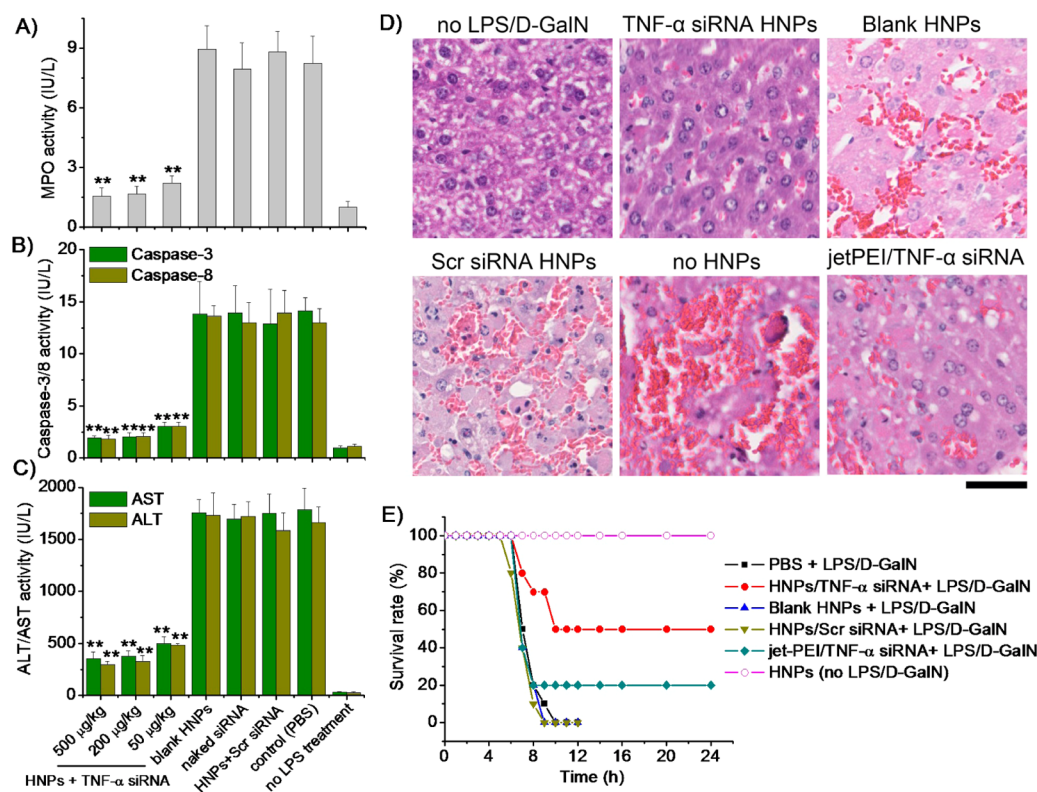


Figure 5. Systemically administered HNP containing TNF- α siRNA HNP mediate anti-inflammatory effect against LPS/D-GalN-induced hepatic failure. MPO levels in the mouse liver homogenate (A), hepatic caspase-3/8 levels (B), and serum ALT and AST levels (C) 5 h after LPS/D-GalN stimulation ($n = 4$). (D) HE-stained liver sections from mice receiving HNP at 50 μ g of siRNA/kg. Liver tissues were harvested 5 h after LPS/D-GalN stimulation (scale bar = 50 μ m). (E) Survival of mice following i.v. injection of HNP (50 μ g siRNA/kg) and i.p. injection of LPS/D-GalN 24 h later ($n = 10$).

HNP-mediated TNF- α silencing. For instance, LPS receptor CD14 participates in the release of TNF- α in LPS-stimulated RAW 264.7 cells and PECs but not in Kupffer cells.⁴⁶ More comparison studies on the biological effect of HNP toward RAW 264.7 cells/PECs and Kupffer cells are necessary in future studies.

The ability of PPABLG HNP to enhance the delivery of TNF- α siRNA *in vivo* was then investigated in a mouse model of LPS/D-galactosamine (D-GalN)-induced acute liver failure. In this model, GalN blocks gene transcription in the liver, and LPS in turn induces an acute, cytokine-dependent hepatic inflammation accompanied by massive liver apoptosis and death.⁴⁷ A key requirement for the successful delivery of siRNA *in vivo* is protection of the siRNA from serum nucleases. Thus, we first evaluated the siRNA stability following serum treatment. As shown in Figure S20, free siRNA was almost degraded upon 2 h treatment, evidenced by the disappearance of the siRNA band after agarose gel electrophoresis. Comparatively, siRNA encapsulated in HNP preserved its integrity, which could be attributed to the restricted access of nucleases toward the siRNA molecules. The *in vivo* efficacy of nonviral siRNA delivery vectors is also closely related to the systemic distribution and translocation. As such, we also explored the biodistribution profiles of i.v.-administered HNP containing DY800-siRNA (Figure 4A). Two hours after i.v. administration, the PPABLG HNP carrying DY800-siRNA were largely accumulated in macrophage-enriched organs, such as liver, spleen, and lung. An appreciable amount of DY800-siRNA was also found in kidney and bladder, which could be related to the renal clearance of HNP that might disassemble

in the glomerular basement membrane.⁴⁸ siRNA distribution in the intestine was also noted, which suggested that it may have been translocated to the intestinal circulation and possibly be excreted *via* stool. Higher siRNA distribution level in systemic organs was noted for HNP compared to free siRNA, which could be due to the rapid elimination of free siRNA from the body upon systemic delivery. The relatively low siRNA level in the liver while higher level in the intestine might be attributed to the fast metabolism of free siRNA in the liver, which was rapidly transferred to the gallbladder and thereafter the intestine, where it could get cleared *via* stool. Because liver macrophages (Kupffer cells) are the target cells for HNP-mediated *in vivo* TNF- α silencing, we further explored whether Kupffer cells can effectively take up the PPABLG HNP after i.v. administration. In the liver sections stained with FITC-F4/80, it was shown that Cy3-siRNA carried by HNP was mainly taken up by FITC-F4/80-stained Kupffer cells while only a small amount of the Cy3-siRNA was located in other unstained cells or in the intercellular compartment (Figure S21), indicating effective delivery of siRNA to Kupffer cells. In accordance with the accumulation of HNP in macrophage-enriched organs, i.v. injection of PPABLG HNP (PPABLG/PAOBLG-MPA/siRNA = 20/2/1, w/w/w) at TNF- α siRNA doses of 500, 200, and 50 μ g of siRNA/kg markedly attenuated the TNF- α mRNA levels in liver, spleen, and lung (Figure 4B), and thus they reduced LPS/D-GalN-induced serum TNF- α production by 94, 93, and 86%, respectively (Figure 4C). As controls, HNP carrying Scr siRNA or naked siRNA exerted an unappreciable gene-silencing effect. These results collectively indicated that i.v.-administered HNP were effectively trans-

ferred to macrophages in the reticuloendothelial tissues to mediate systemic TNF- α depletion. Because TNF- α contributes to the induction of pro-inflammatory mediators such as interleukin-1 β (IL-1 β) and interleukin-6 (IL-6) during the LPS-triggered inflammatory cascade, we further investigated whether HNP-mediated TNF- α knockdown could also lead to the suppression of these cytokines. As illustrated in Figure 4D, serum IL-1 β and IL-6 levels were reduced by 76 and 81%, respectively, following administration of PPABLG HNPs at 500 μ g of TNF- α siRNA/kg. The innate inflammatory responses and immune effects based on the interaction with siRNA and Toll-like receptor (TLR)-3, -7, and -8 should be excluded for a clinically applicable siRNA delivery system.⁴⁹ The induction of pro-inflammatory cytokines (such as IFN- γ) via siRNA interaction with endosomal TLR-3, -7, and -8 is often potentiated by conventional nonviral carriers that experience CME and endosomal/lysosomal entrapment.⁴⁹ However, for the PPABLG HNPs, serum IFN- γ levels were not significantly increased 2 h after i.v. administration (500 μ g of siRNA/kg, Figure S22). It therefore indicated that PPABLG HNPs would not activate pro-inflammatory cytokines or induce IFN- γ responses *in vivo*, which could be closely related to their non-endocytic internalization kinetics and potent capability in avoiding endosomal/lysosomal entrapment.

Because TNF- α is a critical mediator of the hepatic inflammatory cascade, we were thus motivated to explore whether the HNP-mediated inhibition of TNF- α production would afford protection against hepatic injury induced by LPS/D-GalN. Mice challenged by LPS/D-GalN experienced various pathologic symptoms toward inflammation, including a notable increase in the hepatic level of myeloperoxidase (MPO) that indicated neutrophil infiltration (Figure 5A), an elevation in the hepatic levels of caspase-3 and caspase-8 that mediated signaling cascade during hepatocyte apoptosis (Figure 5B),⁵⁰ and an augment in the serum aspartate amino transferase (AST) and alanine amino transferase (ALT) levels as biomarkers for liver damage (Figure 5C). Necropsy examination revealed that livers of LPS/D-GalN-treated mice turned black, indicating severe lipid accumulation, liver steatosis, and hemorrhage. Histological observation on HE-stained liver sections also revealed remarkable inflammatory traces, including a congested central vein, infiltrated inflammatory cells, disarranged hepatocytes, and broken cytolemma (Figure 5D). In comparison, mice receiving i.v. administration of PPABLG HNPs 24 h before LPS/D-GalN stimulation demonstrated significantly improved therapeutic outcomes, evidenced by the reduced hepatic caspase-3/8 levels, hepatic MPO level, and serum AST/ALT levels (Figure 5A–C). The livers remained a normal reddish color, and the inflammatory symptoms in the HE-stained liver tissues were also notably alleviated (Figure 5D). As a result, LPS/D-GalN-induced animal lethality was suppressed to achieve a survival rate of 50% at the TNF- α siRNA dose of 50 μ g/kg within the observation period of 10 days, significantly outperforming jet-PEI as a commercially available gene delivery vector (20% survival, Figure 5E).

Safety is an important aspect of nanomaterials, which should be taken into consideration for clinical application. Thus, MTT assays were first adopted to evaluate the cytotoxicity of PPABLG HNPs in RAW 264.7 cells. As shown in Figure S18, negligible cytotoxicity was observed at the final siRNA concentrations of 12 μ g/mL (4 h incubation) and 5 μ g/mL (24 h incubation). When the PPABLG HNPs were i.v.-injected, they were extensively diluted by the blood and other

physiological fluid (by at least 7–14-fold) to reach a final concentration of approximately 2–4 μ g/mL. It was therefore anticipated that they would not induce notable cytotoxicity *in vivo*. In support of such deduction, the percentage level of Kupffer cells in liver cells was not significantly altered following administration of HNPs at 500 μ g of siRNA/kg (Figure S24), which suggested that the PPABLG HNPs did not induce appreciable toxicity to Kupffer cells, where they mediate TNF- α gene silencing. A hemolytic study as well as histological observation was also performed to primarily evaluate the biocompatibility of PPABLG HNPs. As shown in Figure S23, the hemolysis ratio of PPABLG HNPs at the polypeptide concentration of \leq 50 μ g/mL was below 5%, suggesting its desired compatibility when systemically injected. In the HE-stained tissue cross sections of major organs (Figure S25), no necrosis, inflammation, edema, or other pathological signs were detected after i.v. administration of PPABLG HNPs (500 μ g of siRNA/kg), except for a slight inflammation in the lung, indicating minimal acute toxicity of the nanoparticles.

Lack of immune toxicity is also important for a siRNA delivery system. Therefore, we further evaluated the effect of PPABLG HNPs on immune cells such as leukocytes and on TLR-4 activation. As shown in Table S3, i.v. administration of PPABLG HNPs at 500 μ g of siRNA/kg did not appreciably change the leukocyte number or their differential counting. Because TLR-4 activation induces both Th1 cytokines (IL-12, TNF- α , and IFN- γ) and type I interferon,⁵¹ we further evaluated the serum cytokine levels following PPABLG HNP treatment. As shown in Figure S22, i.v. administration of PPABLG HNPs at 500 μ g of siRNA/kg did not lead to appreciable production of TNF- α , IFN- α , IFN- γ , or IL-12, which primary indicated their low immune toxicities.

CONCLUSION

We developed a membrane-penetrating polypeptide-based hybrid nanocarrier that mediates effective TNF- α siRNA delivery *in vitro* and *in vivo*. The helical structure of the polypeptide features pore formation on cellular and endosomal membranes to facilitate the cellular internalization as well as endosomal escape of the siRNA cargo in macrophages. Consequently, HNPs containing TNF- α siRNA afforded effective systemic downregulation of TNF- α following systemic administration at a low dose of 50 μ g/kg and thus demonstrated a potent anti-inflammatory effect to rescue animals from LPS/D-GalN-induced hepatic sepsis. These unique properties of PPABLG HNPs rendered their promising applications for anti-inflammation therapies.

MATERIALS AND METHODS

Materials, Cells, and Animals. All chemicals were purchased from Sigma-Aldrich (St. Louis, MO, USA) and used as received unless otherwise specified. Anhydrous tetrahydrofuran, hexane, and dimethylformamide (DMF) were dried by a column packed with 4 Å molecular sieves and stored in a glovebox. Dry nitrobenzene (NB) was prepared by treating regular NB with CaH₂ followed by distillation under reduced pressure. HMDS and 1,5,7-triazabicyclo[4.4.0]dec-5-ene were dissolved in DMF in a glovebox. VB-L-glu-NCA was synthesized according to published literature.^{36,37} Lipofectamine 2000 (LFP2000) and 3-(4,5-dimethylthiazol-2-yl)-2,5-diphenyl-2H-tetrazolium bromide (MTT) were purchased from Invitrogen (Carlsbad, CA, USA). Lipidoid (structure shown in Scheme S3) was synthesized as described previously.⁴⁵ Spectra/Por RC dialysis tubing with a molecular weight cutoff (MWCO) of 1 kDa was purchased from Spectrum Laboratories (Rancho Dominguez, CA, USA). TNF- α

siRNA duplex and negative control siRNA containing scrambled sequences were supplied by Integrated DNA Technologies (Coralville, IA, USA) and dissolved in diethylpyrocarbonate (DEPC)-treated water before use. The siRNA sequences are shown in Table S1. Cy3-labeled or FAM-labeled TNF- α siRNA duplex (Cy3-siRNA or FAM-siRNA, purchased from Dharmacon Research Inc.) was used for *in vitro* cell uptake studies, while DY800-labeled TNF- α siRNA duplex (DY800-siRNA, purchased from Dharmacon Research Inc.) was used for the *in vivo* biodistribution study.

RAW 264.7 cells (mouse monocyte macrophage) were purchased from the American Type Culture Collection (Rockville, MD, USA) and cultured in DMEM supplemented with 10% FBS.

Male C57BL/6 mice (8–10 wk) were obtained from Shanghai Slaccas Experimental Animal Co., Ltd. (Shanghai, China) and were housed in a clean room, four to a cage, with access to water *ad libitum*, a 12:12 h light–dark cycle (7:00 am–7:00 pm), and a temperature of 25 ± 1 °C. The animal experimental protocols were reviewed and approved by the Institutional Animal Care and Use Committee, Soochow University.

Synthesis and Characterization of PPBLG. VB-L-Glu-NCA was prepared as described previously.^{37,52} PPBLG was synthesized *via* ring-opening polymerization (ROP) of VB-L-Glu-NCA as initiated by HMDS followed by multistep side-chain derivatization.^{36,37} Briefly, in a glovebox, VB-L-Glu-NCA (120 mg, 0.415 mmol) was dissolved in a mixture of DMF (1.0 mL) and nitrobenzene (30 μ L), followed by addition of HMDS (41.5 μ L, 0.1 mol/L, M/I = 100) solution in DMF. The reaction mixture was stirred at room temperature for 48 h (monomer conversion >99%) to obtain poly(γ -(4-vinylbenzyl)-L-glutamate) (PVBLG). Benzyl chloroformate (100 μ L) and *N,N*-diisopropylethylamine (100 μ L) were added to cap the amino end groups, and DMF was removed under vacuum. PVBLG was precipitated using cold ether and collected by centrifugation. The degree of polymerization (DP) of PVBLG was 205 with a narrow PDI value of 1.08 as determined by GPC. PVBLG (100 mg) was then dissolved in chloroform (60 mL) and oxidized by O₃ at –78 °C for 3 min. Dimethyl sulfide (1.0 mL) was then added, and the solution was stirred at room temperature overnight, followed by removal of the solvent under vacuum. The product was precipitated by methanol and collected by centrifugation. It then reacted with 1-(2-aminoethyl)-piperidine (440 μ L) in DMF (4 mL) at 50 °C for 24 h; borane pyridine (390 μ L) was added, and the solution was stirred at 50 °C for another 24 h; 5 mol/L HCl (2 mL) was added and stirred for 10 min. The final product PPBLG was then dialyzed against DI water (MWCO = 1 kDa) and lyophilized. PPABDLG as a random-coiled analogue of PPBLG was polymerized from the racemic VB-D,L-Glu-NCA^{37,52} with a DP of 214 and PDI value of 1.06.

Synthesis and Characterization of PAOBLG-MPA. AOB-L-Glu-NCA PAOBLG-MPA was synthesized *via* ROP of AOB-L-Glu-NCA as initiated by HMDS followed by the thiol-ene “click” chemistry. Briefly, in a glovebox, AOB-L-Glu-NCA (32 mg, 0.1 mmol) was dissolved in DMF (1 mL), followed by addition of HMDS (20 μ L, 2 μ mol) in DMF. The solution was stirred for 16 h at room temperature until monomer conversion reached 99%. PAOBLG was then precipitated with ether (15 mL) and washed with ether three times. The polymer was then collected by centrifugation and dried under vacuum. The DP of PAOBLG was 53 with a narrow PDI value of 1.05 as determined by GPC. To obtain PAOBLG-MPA, PAOBLG (16 mg, 0.06 mmol), 2-aminoethanethiol hydrochloride (34 mg, 0.3 mmol), and Irgacure2959 photoinitiator (1 mg, 0.004 mmol) were dissolved in DMF/DI water (1.0 mL/0.1 mL) in a quartz bottle that was sealed with a rubber septum. The mixture was purged with N₂ for 10 min and irradiated with a 365 nm UV lamp (16 mW/cm²) for 10 min. The crude product was dialyzed against water for 2–3 days and lyophilized. The modification efficiency was determined to be about 100% based on ¹H NMR analysis (Figure S3). Circular dichroism measurement of polypeptides was carried out on a JASCO J-700 CD spectrometer. Polypeptide aqueous solution was prepared at the concentration of 0.1 mg/mL, and the solution was placed in a quartz cell with a path length of 0.2 cm. The mean residue molar ellipticity of each polymer was calculated based on the measured apparent ellipticity by following the

reported formulas: ellipticity ($[\theta]$ in deg·cm²·dmol^{–1}) = (millidegrees \times mean residue weight)/(path length in millimeters \times concentration of polypeptide in mg mL^{–1}). The helicity of the polypeptides was calculated by the following equation: helicity = ($-\theta_{222} + 3000$)/39000. To measure the CD spectra of polypeptide/siRNA complexes, PPBLG and siRNA were separately dissolved in DI water at 0.1 mg/mL and mixed at 20:1 (w/w) before incubation at room temperature for 20 min and CD measurement.

Preparation and Characterization of HNPs. PPBLG, PAOBLG-MPA, and siRNA were separately dissolved in pH 7.2 HEPES (20 mM, containing 150 mM NaCl, prepared using DEPC-treated water) at 1, 0.2, and 0.2 mg/mL, respectively. PAOBLG-MPA and siRNA were mixed at various weight ratios of 20, 10, 8, 6.7, 5, 4, 2.7, 2, 1.6, and 1.3, into which PPBLG was quickly added at the constant PPBLG/siRNA weight ratio of 20:1 (equal to PPBLG/PAOBLG-MPA weight ratios of 1, 2, 2.5, 3, 4, 5, 7.5, 10, 12.5, and 15, respectively). The mixture was vortexed for 10 s and further incubated at 37 °C for 20 min to allow complete complexation. The obtained HNPs were characterized for size and ζ -potential using dynamic light scattering (Zetasizer Nano-ZS, Malvern). A gel retardation assay was used to evaluate siRNA condensation. Briefly, HNPs or naked siRNA were loaded in 4% low-melting agarose gel (200 ng siRNA/well) followed by electrophoresis at 56 V for 1 h and visualization of siRNA migration using the gel documentation. To determine the siRNA encapsulation efficiency, an ethidium bromide (EB) exclusion assay was adopted.⁵³ Briefly, EB solution was added to the HNPs at a siRNA/EB ratio of 10:1 (w/w), and the mixture was incubated at room temperature for 60 min before quantification of fluorescence intensity on a microplate reader ($\lambda_{\text{ex}} = 510$ nm, $\lambda_{\text{em}} = 590$ nm). A pure EB solution and the siRNA/EB solution were used as negative and positive controls, respectively. The siRNA condensation efficiency (%) was defined as

$$\text{siRNA condensation efficiency (\%)} = \left(1 - \frac{F - F_{\text{EB}}}{F_0 - F_{\text{EB}}} \right) \times 100$$

where F_{EB} and F_0 denote the fluorescence intensity of pure EB solution and the siRNA/EB, respectively. To observe the morphology of HNPs, freshly prepared HNPs were dripped onto a silicon chip, dried at room temperature, and coated with gold before observation by scanning electron microscopy (4800, Hitachi, Japan).

Stability of HNPs and siRNA. In order to evaluate the stability of HNPs against salt and dilution, they were diluted with PBS (0.15 M, pH 7.0) 10-fold before measurement of particle size and ζ -potential using the Zetasizer.

The stability of siRNA against mouse serum was evaluated using gel electrophoresis. Briefly, HNPs (PPBLG/PAOBLG-MPA/siRNA = 20/2/1, w/w/w) or naked siRNA (140 μ L, containing 10 μ g of siRNA) were incubated with mouse serum (0.2 mL) at 37 °C for 2 h, and the mixture was heated at 80 °C for 5 min to inactivate the nucleases. Heparin (1000 U/mL) was then added to dissociate the siRNA, and the mixture was loaded on 4% agarose gel (400 ng siRNA/well) followed by electrophoresis at 56 V for 1 h. The integrity of siRNA was visualized by gel documentation.

Cell Uptake and Intracellular Kinetics. RAW 264.7 cells were seeded on 24-well plates at 5×10^4 cells/well and cultured for 24 h. The medium was replaced by serum-free DMEM (500 μ L) into which FAM-siRNA-containing HNPs (PPBLG/PAOBLG-MPA/siRNA = 20/2/1, w/w/w) were added (0.2 μ g of siRNA/mL). After incubation at 37 °C for 4 h, cells were washed with cold PBS containing heparin (20 IU/mL) three times and subjected to flow cytometry analysis. Cells without HNP treatment served as the blank. To further quantify the cell uptake level, cells were lysed with the RIPA lysis buffer (500 μ L); the quantity of FAM-siRNA in the lysate was determined by spectrofluorimetry ($\lambda_{\text{ex}} = 488$ nm, $\lambda_{\text{em}} = 520$ nm), and the total protein content was determined by the BCA assay. Uptake level was expressed as the amount of FAM-siRNA per milligram of cellular protein. To visualize the uptake and intracellular distribution of HNPs by CLSM, RAW 264.7 cells were seeded on coverslips (1.5 \times 1.5 cm) in a 6-well plate at the density of 2×10^4 cells/well and cultured for 24 h. HNPs

formed from rhodamine-labeled PPABLG and FAM-siRNA were then added (1 μg of siRNA/well, 2 mL media/well) and incubated with RAW 264.7 cells in serum-free DMEM at 37 °C for different times. After being washed with cold heparin–PBS three times, cells were stained with Hoechst33258 (nuclei staining) and observed by CLSM (700, Zeiss, Germany).

To explore the mechanisms involved in the uptake process, cells were preincubated with endocytic inhibitors including NaN_3 (200 mM)/deoxyglucose (50 mM), chlorpromazine (10 $\mu\text{g}/\text{mL}$), genistein (200 $\mu\text{g}/\text{mL}$), methyl- β -cyclodextrin ($\text{m}\beta\text{CD}$, 50 μM), and wortmannin (50 nM) for 30 min prior to addition of FAM-siRNA-containing HNP and throughout the 0.5 or 2 h uptake experiment at 37 °C. Results were expressed as percentage uptake level in control cells that were incubated with HNPs at 37 °C for 0.5 or 2 h. To further explore the caveolae-mediated endocytic pathway, RAW 264.7 cells were co-incubated with Cy3-siRNA-containing HNPs and FITC-CTB (5 $\mu\text{g}/\text{mL}$) for 2 h before CLSM observation. To probe the clathrin-mediated endocytic pathway, RAW 264.7 cells were incubated with Cy3-siRNA-containing HNPs and transferrin-Alexa Fluor 647 (10 $\mu\text{g}/\text{mL}$) for 2 h before CLSM observation.

Polypeptide-induced pore formation on cell membranes was evaluated in terms of the cell uptake of a hydrophilic, membrane-impermeable dye, fluorescein isothiocyanate (FITC) in its nonreactive form (fluorescein–tris(hydroxymethyl)methanethiourea, FITC–Tris).⁴¹ Briefly, RAW 264.7 cells were seeded on 24-well plates at 5×10^4 cells/well and cultured for 24 h. The medium was replaced with serum-free DMEM, and free PPABLG or PPABLG HNPs were added at 2 μg of PPABLG/well, and FITC–Tris was added at 0.4 $\mu\text{g}/\text{well}$. Cells treated with only FITC–Tris served as the control. Following incubation at 37 °C for 2 h, cells were washed with heparin-containing cold PBS three times and lysed with the RIPA lysis buffer. The uptake level of FITC–Tris in the lysate was quantified by spectrofluorimetry, while the protein level was determined using the BCA kit. Results were expressed as nanograms of FITC–Tris associated with 1 mg of cellular protein.

The endosomal entrapment and escape of HNPs were evaluated by CLSM. Briefly, RAW 264.7 cells were incubated with FAM-siRNA-containing HNPs (0.1 μg of siRNA/mL) at 37 °C for different times. Cells were then washed with cold PBS containing heparin (20 IU/mL) three times, and the endosomal/lysosomal compartments were stained with LysoTracker Red (Invitrogen) according to the manufacturer's protocol. After being nuclei-stained with Hoechst33258, cells were observed by CLSM (Zeiss-700, Germany). To quantify the FAM-siRNA release from RhB-polypeptide or endosomal escape ratio of FAM-siRNA, the colocalization ratio between FAM-siRNA and RhB-polypeptide or LysoTracker Red was quantified as follows using the ImageJ software.⁵⁴

$$\text{colocalization ratio (\%)} = \frac{\text{FAM pixels}_{\text{colocalization}}}{\text{FAM pixels}_{\text{total}}} \times 100$$

where $\text{FAM pixels}_{\text{colocalization}}$ represents the number of FAM pixels colocalizing with RhB-polypeptide or LysoTracker Red, and $\text{FAM pixels}_{\text{total}}$ represents the number of all FAM pixels in the CLSM images. Results were presented as the mean of 20 individual cells.

Cytotoxicity of SSNPs. RAW 264.7 cells were seeded on 96-well plate at 1×10^4 cells/well and cultured for 24 h before media replacement with serum-free DMEM (100 $\mu\text{L}/\text{well}$). HNPs (PPABLG/PAOBLG-MPA/siRNA = 20/2/1, w/w/w) were added at the siRNA amount of 0.1, 0.2, 0.5, 1, 2, and 5 $\mu\text{g}/\text{well}$ (equal to final siRNA concentrations of 1, 1.9, 4.2, 7.4, 11.8, and 18.1 $\mu\text{g}/\text{mL}$, respectively). Following incubation for 4 h, the medium was removed and serum-containing DMEM was added. Cells were further cultured for 20 h before viability assessment by the MTT assay.

In Vitro TNF- α Silencing in Macrophages. RAW 264.7 cells were seeded on a 24-well plate at 5×10^4 cells/well and cultured for 24 h. The medium was changed to serum-free DMEM, and siRNA-containing HNPs (PPABLG/PAOBLG-MPA/siRNA = 20/2/1, w/w/w) were added at various siRNA concentrations. Following incubation at 37 °C for 4 h, the medium was replaced by serum-containing

DMEM, and cells were further cultured for 20 h before LPS stimulation (100 ng·mL⁻¹) for 3 h. Extracellular TNF- α production was quantified by ELISA (R&D Systems, MN, USA), and TNF- α mRNA level was monitored by real-time PCR. The silencing efficiency was denoted as the percentage of TNF- α or TNF- α mRNA levels of the control cells, which did not receive treatment with HNPs. To prepare samples for real-time PCR analysis, RNA was isolated from cells using the Trizol reagent (Invitrogen). cDNA was synthesized from 500 ng of total RNA using the high-capacity cDNA reverse transcription kit (Applied Biosystems, Carlsbad, CA, USA) according to the manufacturer's instructions. Synthesized cDNA, TNF- α primers (forward and reverse), and SYBR Premix Ex Taq were mixed and run on the ABI PRISM 7900HT real-time PCR system (Applied Biosystems, Carlsbad, CA, USA). Sequences of the primers used were designed with Primer Bank (Table S2). The ribosomal mRNA actin was used as an internal loading control, and its expression did not change over the 24 h period following addition of LPS, HNPs, or siRNA.

To evaluate RNAi in primary macrophages, murine PECs were collected and treated as follows. Briefly, male C57BL/6 mice were sacrificed, and 1 mL of DMEM containing 10% FBS was intraperitoneally injected. The abdominal fluids were extracted and centrifuged at 1000 rpm for 5 min, and the collected PECs were seeded on a 96-well plate at 5×10^4 cells/well and cultured in DMEM supplemented with 10% FBS. The cells were allowed to adhere for 2 h before the medium was replaced by fresh DMEM containing 10% FBS to remove unadherent cells. HNPs were then added and incubated with cells for 4 h under serum-containing conditions followed by further incubation for 20 h and LPS stimulation as described above. TNF- α and TNF- α mRNA levels were quantified by ELISA and real-time PCR, respectively, as described above.

Biodistribution of HNPs Following Intravenous Injection. To evaluate biodistribution profiles of systemically administered HNPs, DY800-siRNA-containing HNPs (PPABLG/PAOBLG-MPA/siRNA = 20/2/1, w/w/w) or naked DY800-siRNA were i.v.-injected to mice at 200 μg of siRNA/kg (three mice per group). Mice were sacrificed 2 h after administration, and major organs including liver, spleen, lung, heart, kidney, bladder, brain, stomach, small intestine, and large intestine were harvested, washed with PBS, fixed in 10% formalin, and put in a 24-well plate before quantification of the fluorescent intensity in each organ using an Odyssey infrared mouse imaging system (800 nm emission, LI-COR, Lincoln, NE, USA) as described previously.⁵⁵ Tissues harvested from animals that did not receive HNPs or siRNA administration served as the blank, and their fluorescence intensity was subtracted from test tissues. We first made the calibration curve by measuring the fluorescence intensities of siRNA solutions (10 $\mu\text{L}/\text{well}$) placed in the center of a 24-well plate and plotting them against concentrations (0–10 $\mu\text{g}/\text{mL}$, corresponding to a total amount of 0–100 ng). The fluorescence intensity of each organ was compared with the calibration curve to calculate the total amount of DY800-siRNA inside each organ piece, and it was further normalized by the weight of tissues used for the measurement to obtain the biodistribution level in each organ that was represented as nanograms of siRNA per milligram of tissue.

To further probe the distribution of PPABLG HNPs in liver macrophages (Kupffer cells), male C57/BL6 mice (18–20 g) were intravenously injected with Cy3-siRNA-containing PPABLG HNPs at 500 μg of siRNA/kg. Two hours after injection, the liver was harvested and fixed in 4% paraformaldehyde for 4 h, followed by incubation with 30% sucrose overnight. Pretreated liver was embedded in OCT compound and kept frozen at –80 °C. The 10 μm thick cryosections were generated from frozen liver tissues. After being dried overnight in the dark, the cryosections were fixed with acetone at –20 °C for 5 min, washed three times with PBS (5 min \times 3), blocked with PBS containing 5% normal donkey serum for 1 h at room temperature, and then stained with FITC-F4/80 (1:20 dilution) for another 1.5 h at room temperature. After being washed with PBS (8 min \times 3), the cryosections were mounted in Prolong-Gold containing DAPI and observed by CLSM.

In Vivo TNF- α Knockdown via Intravenous Injection of HNPs. TNF- α siRNA-containing HNPs (PPABLG/PAOBLG-MPA/siRNA = 20/2/1, w/w/w) were i.v.-injected into mice at 50, 200, and 500 μg of siRNA/kg (four mice per group), with untreated mice serving as a control group. Twenty-four hours after administration, LPS (100 $\mu\text{g}/\text{kg}$) and D-GalN (1.25 g/kg) were i.p.-injected. Blood was collected 1.5 h later to determine the serum TNF- α , IL-1 β , and IL-6 levels by ELISA.

In another experiment, HNPs were i.v.-injected into mice as described above. Five hours after LPS/D-GalN stimulation (100 $\mu\text{g}/\text{kg}$ and 1.25 g/kg), mice were sacrificed; liver, spleen, and lung were harvested, cut into small pieces, washed with saline, and homogenized with the Trizol reagent. RNA extraction was performed as described for RAW 264.7 cells, and intracellular TNF- α mRNA levels were monitored by real-time PCR.

Anti-inflammatory Efficacy via Intravenous Injection of HNPs. Blood was collected 5 h after LPS/D-GalN challenge, and serum was separated to evaluate the serum ALT as well as AST levels using commercial kits (Biovision Inc., San Francisco, CA, USA). For histological evaluation, mouse liver was also harvested 5 h after LPS/D-GalN stimulation, fixated in paraffin, cross-sectioned, and stained with hematoxylin/eosin (HE). TNF- α -induced hepatic apoptosis was evaluated by assaying the caspase-3 and caspase-8 levels in mouse livers. For lethality tests, mice (10 per group) were i.v.-administered with HNPs (50 μg of siRNA/kg) or PBS. Twenty-four hours later, LPS/D-GalN was i.p.-injected as described above, and animal survival was monitored for 24 h. Mice receiving administration of HNPs with no i.p. injection of LPS/D-GalN served as the control.

Immune Toxicity. To evaluate the immune toxicity of PPABLG HNPs, PPABLG HNPs (PPABLG/PAOBLG-MPA/siRNA = 20/2/1, w/w/w) were i.v.-injected into mice at 500 μg of siRNA/kg. Two hours after injection, blood was harvested from mice and serum was isolated by centrifugation. Whole blood was used for complete blood count analyses (white blood cell count, lymphocyte count, % lymphocyte, monocyte count, % monocyte, granulocyte count, and % granulocyte) on an automatic hematology analyzer, and serum was used for quantification of cytokine (TNF- α , IFN- α , IFN- γ , and IL-12) levels by ELISA. Mice receiving 200 μL of PBS instead of HNPs served as the control.

To probe the potential toxicity of PPABLG HNPs toward Kupffer cells as the target cell for TNF- α siRNA-mediated gene silencing, male C57/BL6 mice (18–20 g) were divided into two groups ($n = 4$), intravenously injected with PPABLG HNPs (500 μg of siRNA/kg) or PBS as the control. Twenty-four hours after injection, mice were perfused with PBS and the livers were collected, digested with DMEM medium containing collagenase (1.5 mg/mL) at 37 $^{\circ}\text{C}$ for 45 min, and passed through a 70 μm nylon cell strainer. After centrifugation at 1300 rpm for 5 min, two million cells were resuspended and washed with flow buffer and then blocked with rat anti-mouse CD16/32 antibody at 4 $^{\circ}\text{C}$ for 5 min. PE-Cy7 CD45, APC-Gr1, APC-Cy CD11b, and FITC-F4/80 were used to stain Kupffer cells, and the percentage level of Kupffer cells was measured on a Gallios flow cytometer and analyzed with Kaluza software (Beckman).

Statistical Analysis. Statistical analysis was performed using a Student's t test, and differences were judged to be significant at $*p < 0.05$ and $**p < 0.01$.

ASSOCIATED CONTENT

Supporting Information

The Supporting Information is available free of charge on the ACS Publications website at DOI: 10.1021/acsnano.5b05470.

Additional experimental details (PDF)

AUTHOR INFORMATION

Corresponding Author

*E-mail: lcyin@suda.edu.cn.

Notes

The authors declare no competing financial interest.

ACKNOWLEDGMENTS

We would like to acknowledge the support from the National Natural Science Foundation of China (51403145 and 51573123), the Science and Technology Department of Jiangsu Province (BK20140333), Collaborative Innovation Center of Suzhou Nano Science & Technology, and Priority Academic Program Development of Jiangsu Higher Education Institutions (PAPD), and National Science Foundation (CHE 1508710).

REFERENCES

- (1) Ye, C. T.; Choi, J. G.; Abraham, S.; Wu, H. Q.; Diaz, D.; Terreros, D.; Shankar, P.; Manjunath, N. Human Macrophage and Dendritic Cell-Specific Silencing of High-Mobility Group Protein B1 Ameliorates Sepsis in a Humanized Mouse Model. *Proc. Natl. Acad. Sci. U. S. A.* **2012**, *109*, 21052–21057.
- (2) Un, K.; Kawakami, S.; Yoshida, M.; Higuchi, Y.; Suzuki, R.; Maruyama, K.; Yamashita, F.; Hashida, M. Efficient Suppression of Murine Intracellular Adhesion Molecule-1 Using Ultrasound-Responsive and Mannose-Modified Lipoplexes Inhibits Acute Hepatic Inflammation. *Hepatology* **2012**, *56*, 259–269.
- (3) Nie, H.; Zheng, Y. X.; Li, R. S.; Guo, T. B.; He, D. Y.; Fang, L.; Liu, X. B.; Xiao, L. B.; Chen, X.; Wan, B.; et al. Phosphorylation of FOXP3 Controls Regulatory T Cell Function and Is Inhibited by TNF- α in Rheumatoid Arthritis. *Nat. Med.* **2013**, *19*, 322–328.
- (4) Kirman, I.; Whelan, R. L.; Nielsen, O. H. Infliximab: Mechanism of Action Beyond TNF- α Neutralization in Inflammatory Bowel Disease. *Eur. J. Gastroenterol. Hepatol.* **2004**, *16*, 639–641.
- (5) Keane, J.; Gershon, S.; Wise, R. P.; Mirabile-Levens, E.; Kasznica, J.; Schwieterman, W. D.; Siegel, J. N.; Braun, M. M. Tuberculosis Associated with Infliximab, a Tumor Necrosis Factor (α)-Neutralizing Agent. *N. Engl. J. Med.* **2001**, *345*, 1098–1104.
- (6) Davis, M. E.; Zuckerman, J. E.; Choi, C. H. J.; Seligson, D.; Tolcher, A.; Alabi, C. A.; Yen, Y.; Heide, J. D.; Ribas, A. Evidence of RNAi in Humans from Systemically Administered siRNA via Targeted Nanoparticles. *Nature* **2010**, *464*, 1067–1070.
- (7) Lee, H.; Lytton-Jean, A. K. R.; Chen, Y.; Love, K. T.; Park, A. I.; Karagiannis, E. D.; Sehgal, A.; Querbes, W.; Zurenko, C. S.; Jayaraman, M.; et al. Molecularly Self-Assembled Nucleic Acid Nanoparticles for Targeted *In Vivo* siRNA Delivery. *Nat. Nanotechnol.* **2012**, *7*, 389–393.
- (8) Woodrow, K. A.; Cu, Y.; Booth, C. J.; Saucier-Sawyer, J. K.; Wood, M. J.; Saltzman, W. M. Intravaginal Gene Silencing using Biodegradable Polymer Nanoparticles Densely Loaded with Small-Interfering RNA. *Nat. Mater.* **2009**, *8*, 526–533.
- (9) Lee, S. J.; Huh, M. S.; Lee, S. Y.; Min, S.; Lee, S.; Koo, H.; Chu, J. U.; Lee, K. E.; Jeon, H.; Choi, Y.; et al. Tumor-Homing Poly-siRNA/Glycol Chitosan Self-Cross-Linked Nanoparticles for Systemic siRNA Delivery in Cancer Treatment. *Angew. Chem., Int. Ed.* **2012**, *51*, 7203–7207.
- (10) Dassie, J. P.; Liu, X. Y.; Thomas, G. S.; Whitaker, R. M.; Thiel, K. W.; Stockdale, K. R.; Meyerholz, D. K.; McCaffrey, A. P.; McNamara, J. O.; Giangrande, P. H. Systemic Administration of Optimized Aptamer-siRNA Chimeras Promotes Regression of PSMA-Expressing Tumors. *Nat. Biotechnol.* **2009**, *27*, 839–846.
- (11) Wei, H.; Schellinger, J. G.; Chu, D. S. H.; Pun, S. H. Neuron-Targeted Copolymers with Sheddable Shielding Blocks Synthesized Using a Reducible, RAFT-ATRP Double-Head Agent. *J. Am. Chem. Soc.* **2012**, *134*, 16554–16557.
- (12) Kozielski, K. L.; Tzeng, S. Y.; De Mendoza, B. A. H.; Green, J. J. Bioreducible Cationic Polymer-Based Nanoparticles for Efficient and Environmentally Triggered Cytoplasmic siRNA Delivery to Primary Human Brain Cancer Cells. *ACS Nano* **2014**, *8*, 3232–3241.
- (13) Tranter, M.; Liu, Y. M.; He, S. W.; Gulick, J.; Ren, X. P.; Robbins, J.; Jones, W. K.; Reineke, T. M. *In Vivo* Delivery of Nucleic Acids via Glycopolymer Vehicles Affords Therapeutic Infarct Size Reduction *In Vivo*. *Mol. Ther.* **2012**, *20*, 601–608.
- (14) Li, J.; Yu, X.; Wang, Y.; Yuan, Y.; Xiao, H.; Cheng, D.; Shuai, X. A Reduction and pH Dual-Sensitive Polymeric Vector for Long-

Circulating and Tumor-Targeted siRNA Delivery. *Adv. Mater.* **2014**, *26*, 8217–8224.

(15) Nelson, C. E.; Kim, A. J.; Adolph, E. J.; Gupta, M. K.; Yu, F.; Hocking, K. M.; Davidson, J. M.; Guelcher, S. A.; Duvall, C. L. Tunable Delivery of siRNA from a Biodegradable Scaffold to Promote Angiogenesis *In Vivo*. *Adv. Mater.* **2014**, *26*, 607–614.

(16) Howard, K. A.; Paludan, S. R.; Behlke, M. A.; Besenbacher, F.; Deleuran, B.; Kjems, J. Chitosan/siRNA Nanoparticle-mediated TNF- α Knockdown in Peritoneal Macrophages for Anti-inflammatory Treatment in a Murine Arthritis Model. *Mol. Ther.* **2009**, *17*, 162–168.

(17) Kim, S. S.; Ye, C. T.; Kumar, P.; Chiu, L.; Subramanya, S.; Wu, H. Q.; Shankar, P.; Manjunath, N. Targeted Delivery of siRNA to Macrophages for Anti-inflammatory Treatment. *Mol. Ther.* **2010**, *18*, 993–1001.

(18) Wilson, D. S.; Dalmaso, G.; Wang, L. X.; Sitaraman, S. V.; Merlin, D.; Murthy, N. Orally Delivered Thioketal Nanoparticles Loaded with TNF- α -siRNA Target Inflammation and Inhibit Gene Expression in the Intestines. *Nat. Mater.* **2010**, *9*, 923–928.

(19) Lee, S.; Yang, S. C.; Kao, C. Y.; Pierce, R. H.; Murthy, N. Solid Polymeric Microparticles Enhance the Delivery of siRNA to Macrophages *In Vivo*. *Nucleic Acids Res.* **2009**, *37*, e145.

(20) Kriegel, C.; Amiji, M. Oral TNF- α Gene Silencing using a Polymeric Microsphere-Based Delivery System for the Treatment of Inflammatory Bowel Disease. *J. Controlled Release* **2011**, *150*, 77–86.

(21) Yang, X. Z.; Du, J. Z.; Dou, S.; Mao, C. Q.; Long, H. Y.; Wang, J. Sheddable Ternary Nanoparticles for Tumor Acidity-Targeted siRNA Delivery. *ACS Nano* **2012**, *6*, 771–781.

(22) Shim, M. S.; Wong, S.; Kwon, Y. J. siRNA as a Conventional Drug in the Clinic? Challenges and Current Technologies. *Drug Discovery Today: Technol.* **2012**, *9*, e167–e173.

(23) Roy, K.; Mao, H. Q.; Huang, S. K.; Leong, K. W. Oral Gene Delivery with Chitosan-DNA Nanoparticles Generates Immunologic Protection in a Murine Model of Peanut Allergy. *Nat. Med.* **1999**, *5*, 387–391.

(24) Zheng, D.; Giljohann, D. A.; Chen, D. L.; Massich, M. D.; Wang, X. Q.; Iordanov, H.; Mirkin, C. A.; Paller, A. S. Topical Delivery of siRNA-Based Spherical Nucleic Acid Nanoparticle Conjugates for Gene Regulation. *Proc. Natl. Acad. Sci. U. S. A.* **2012**, *109*, 11975–11980.

(25) Tezgel, A. O.; Gonzalez-Perez, G.; Telfer, J. C.; Osborne, B. A.; Minter, L. M.; Tew, G. N. Novel Protein Transduction Domain Mimics as Nonviral Delivery Vectors for siRNA Targeting NOTCH1 in Primary Human T cells. *Mol. Ther.* **2013**, *21*, 201–209.

(26) Love, K. T.; Mahon, K. P.; Levins, C. G.; Whitehead, K. A.; Querbes, W.; Dorkin, J. R.; Qin, J.; Cantley, W.; Qin, L. L.; Racie, T.; et al. Lipid-Like Materials for Low-Dose, *In Vivo* Gene Silencing. *Proc. Natl. Acad. Sci. U. S. A.* **2010**, *107*, 1864–1869.

(27) van Asbeck, A. H.; Beyerle, A.; McNeill, H.; Bovee-Geurts, P. H. M.; Lindberg, S.; Verdurmen, W. P. R.; Hällbrink, M.; Langel, Ü.; Heidenreich, O.; Brock, R. Molecular Parameters of siRNA–Cell Penetrating Peptide Nanocomplexes for Efficient Cellular Delivery. *ACS Nano* **2013**, *7*, 3797–3807.

(28) Meade, B. R.; Dowdy, S. F. Enhancing the Cellular Uptake of siRNA Duplexes Following Noncovalent Packaging with Protein Transduction Domain Peptides. *Adv. Drug Delivery Rev.* **2008**, *60*, 530–536.

(29) Ruzza, P.; Calderan, A.; Guiotto, A.; Osler, A.; Borin, G. Tat Cell-Penetrating Peptide Has the Characteristics of a Poly(proline) II Helix in Aqueous Solution and in SDS Micelles. *J. Pept. Sci.* **2004**, *10*, 423–426.

(30) Daniels, D. S.; Schepartz, A. Intrinsically Cell-Permeable Miniature Proteins Based on a Minimal Cationic PPII Motif. *J. Am. Chem. Soc.* **2007**, *129*, 14578–14579.

(31) Stewart, K. M.; Horton, K. L.; Kelley, S. O. Cell-Penetrating Peptides as Delivery Vehicles for Biology and Medicine. *Org. Biomol. Chem.* **2008**, *6*, 2242–2255.

(32) Meade, B. R.; Dowdy, S. F. Exogenous siRNA Delivery Using Peptide Transduction Domains/Cell Penetrating Peptides. *Adv. Drug Delivery Rev.* **2007**, *59*, 134–140.

(33) Gooding, M.; Browne, L. P.; Quinteiro, F. M.; Selwood, D. L. siRNA Delivery: From Lipids to Cell-penetrating Peptides and Their Mimics. *Chem. Biol. Drug Des.* **2012**, *80*, 787–809.

(34) Johnson, R. N.; Chu, D. S. H.; Shi, J.; Schellinger, J. G.; Carlson, P. M.; Pun, S. H. HPMA-Oligolysine Copolymers for Gene Delivery: Optimization of Peptide Length and Polymer Molecular Weight. *J. Controlled Release* **2011**, *155*, 303–311.

(35) Meyer, M.; Philipp, A.; Oskuee, R.; Schmidt, C.; Wagner, E. Breathing Life into Polycations: Functionalization with pH-Responsive Endosomolytic Peptides and Polyethylene Glycol Enables siRNA Delivery. *J. Am. Chem. Soc.* **2008**, *130*, 3272–3273.

(36) Lu, H.; Wang, J.; Bai, Y. G.; Lang, J. W.; Liu, S. Y.; Lin, Y.; Cheng, J. J. Ionic Polypeptides with Unusual Helical Stability. *Nat. Commun.* **2011**, *2*, 206.

(37) Gabrielson, N. P.; Lu, H.; Yin, L. C.; Li, D.; Wang, F.; Cheng, J. J. Reactive and Bioactive Cationic α -Helical Polypeptide Template for Nonviral Gene Delivery. *Angew. Chem., Int. Ed.* **2012**, *51*, 1143–1147.

(38) Katas, H.; Alpar, H. O. Development and Characterisation of Chitosan Nanoparticles for siRNA Delivery. *J. Controlled Release* **2006**, *115*, 216–225.

(39) Zhang, Y. F.; Lu, H.; Lin, Y.; Cheng, J. J. Water-Soluble Polypeptides with Elongated, Charged Side Chains Adopt Ultrastable Helical Conformations. *Macromolecules* **2011**, *44*, 6641–6644.

(40) Tang, D. W.; Yu, S. H.; Ho, Y. C.; Mi, F. L.; Kuo, P. L.; Sung, H. W. Heparinized Chitosan/Poly(γ -glutamic acid) Nanoparticles For Multi-Functional Delivery of Fibroblast Growth Factor and Heparin. *Biomaterials* **2010**, *31*, 9320–9332.

(41) Ter-Avetisyan, G.; Tuennemann, G.; Nowak, D.; Nitschke, M.; Herrmann, A.; Drab, M.; Cardoso, M. C. Cell Entry of Arginine-Rich Peptides Is Independent of Endocytosis. *J. Biol. Chem.* **2009**, *284*, 3370–3378.

(42) Khalil, I. A.; Kogure, K.; Akita, H.; Harashima, H. Uptake Pathways and Subsequent Intracellular Trafficking in Nonviral Gene Delivery. *Pharmacol. Rev.* **2006**, *58*, 32–45.

(43) Zhao, X.; Yin, L.; Ding, J.; Tang, C.; Gu, S.; Yin, C.; Mao, Y. Thiolated Trimethyl Chitosan Nanocomplexes as Gene Carriers with High *In Vitro* and *In Vivo* Transfection Efficiency. *J. Controlled Release* **2010**, *144*, 46–54.

(44) McLendon, P. M.; Fichter, K. M.; Reineke, T. M. Poly-(glycoamidoamine) Vehicles Promote pDNA Uptake through Multiple Routes and Efficient Gene Expression *via* Caveolae-Mediated Endocytosis. *Mol. Pharmaceutics* **2010**, *7*, 738–750.

(45) Akinc, A.; Zumbuehl, A.; Goldberg, M.; Leshchiner, E. S.; Busini, V.; Hossain, N.; Bacallado, S. A.; Nguyen, D. N.; Fuller, J.; Alvarez, R.; et al. A Combinatorial Library of Lipid-Like Materials for Delivery of RNAi Therapeutics. *Nat. Biotechnol.* **2008**, *26*, 561–569.

(46) Lichtman, S. N.; Wang, J.; Lemasters, J. J. LPS Receptor CD14 Participates in Release of TNF- α in RAW 264.7 and Peritoneal Cells but not in Kupffer Cells. *Am. J. Physiol.-Gastr. L* **1998**, *275*, G39–G46.

(47) Park, J. H.; Kim, K. H.; Lee, W. R.; Han, S. M.; Park, K. K. Protective Effect of Melittin on Inflammation and Apoptosis in Acute Liver Failure. *Apoptosis* **2012**, *17*, 61–69.

(48) Zuckerman, J. E.; Choi, C. H. J.; Han, H.; Davis, M. E. Polycation-siRNA Nanoparticles Can Disassemble at the Kidney Glomerular Basement Membrane. *Proc. Natl. Acad. Sci. U. S. A.* **2012**, *109*, 3137–3142.

(49) Sanada, T.; Takaesu, G.; Mashima, R.; Yoshida, R.; Kobayashi, T.; Yoshimura, A. FLN29 Deficiency Reveals Its Negative Regulatory Role in the Toll-like Receptor (TLR) and Retinoic Acid-Inducible Gene I (RIG-I)-Like Helicase Signaling Pathway. *J. Biol. Chem.* **2008**, *283*, 33858–33864.

(50) Nakama, T.; Hirono, S.; Moriuchi, A.; Hasuike, S.; Nagata, K.; Hori, T.; Ido, A.; Hayashi, K.; Tsubouchi, K. Etoposide Prevents Apoptosis in Mouse Liver with D-Galactosamine/Lipopolysaccharide-Induced Fulminant Hepatic Failure Resulting in Reduction of Lethality. *Hepatology* **2001**, *33*, 1441–1450.

(51) Miller, S. I.; Ernst, R. K.; Bader, M. W. LPS, TLR4 and Infectious Disease Diversity. *Nat. Rev. Microbiol.* **2005**, *3*, 36–46.

(52) Lu, H.; Bai, Y. G.; Wang, J.; Gabrielson, N. P.; Wang, F.; Lin, Y.; Cheng, J. J. Ring-Opening Polymerization of Gamma-(4-Vinylbenzyl)-L-Glutamate N-Carboxyanhydride for the Synthesis of Functional Polypeptides. *Macromolecules* **2011**, *44*, 6237–6240.

(53) Yin, L. C.; Tang, H. Y.; Kim, K. H.; Zheng, N.; Song, Z. Y.; Gabrielson, N. P.; Lu, H.; Cheng, J. J. Light-Responsive Helical Polypeptides Capable of Reducing Toxicity and Unpacking DNA: Toward Nonviral Gene Delivery. *Angew. Chem., Int. Ed.* **2013**, *52*, 9182–9186.

(54) Takemoto, H.; Ishii, A.; Miyata, K.; Nakanishi, M.; Oba, M.; Ishii, T.; Yamasaki, Y.; Nishiyama, N.; Kataoka, K. Polyion Complex Stability and Gene Silencing Efficiency with a siRNA-Grafted Polymer Delivery System. *Biomaterials* **2010**, *31*, 8097–8105.

(55) Tang, L.; Fan, T. M.; Borst, L. B.; Cheng, J. J. Synthesis and Biological Response of Size-Specific, Monodisperse Drug-Silica Nanoconjugates. *ACS Nano* **2012**, *6*, 3954–3966.